


RESEARCH ARTICLE

MICROSCOPY  
RESEARCH TECHNIQUE

WILEY

# 2D and 3D immunogold localization on (epoxy) ultrathin sections with and without osmium tetroxide

Jennifer Flechsler<sup>1</sup> | Thomas Heimerl<sup>2</sup> | Carolin Pickl<sup>1</sup> | Reinhard Rachel<sup>3</sup> |  
York-Dieter Stierhof<sup>4</sup> | Andreas Klingl<sup>1</sup> 

<sup>1</sup>Plant Development and Electron Microscopy,  
Department of Biology I, Munchen, Germany

<sup>2</sup>LOEWE Centre for Synthetic Microbiology  
(SYNMIKRO), Philipps-Universität Marburg,  
Marburg, Germany

<sup>3</sup>Institute of Microbiology and Centre for  
Electron Microscopy, University of  
Regensburg, Regensburg, Germany

<sup>4</sup>Microscopy, Center for Plant Molecular  
Biology, University of Tübingen, Tübingen,  
Germany

## Correspondence

Andreas Klingl, Plant Development and  
Electron Microscopy, Department of Biology I,  
Biocenter LMU Munich, Großhaderner Str.  
2-4, 82152 Planegg-Martinsried, Munchen,  
Germany.  
Email: andreas.klingl@biologie.uni-  
muenchen.de

Review Editor: Mingying Yang

## Abstract

For nearly 50 years immunogold labeling on ultrathin sections has been successfully used for protein localization in laboratories worldwide. In theory and in practice, this method has undergone continual improvement over time. In this study, we carefully analyzed circulating protocols for postembedding labeling to find out if they are still valid under modern laboratory conditions, and in addition, we tested unconventional protocols. For this, we investigated immunolabeling of Epon-embedded cells, immunolabeling of cells treated with osmium, and the binding behavior of differently sized gold particles. Here we show that (in contrast to widespread belief) immunolabeling of Epon-embedded cells and of cells treated with osmium tetroxide is actually working. Furthermore, we established a “speed protocol” for immunolabeling by reducing antibody incubation times. Finally, we present our results on three-dimensional immunogold labeling.

## KEYWORDS

(serial) immunogold labeling, Archaea, Diatoms, Epon 812—osmium tetroxide

## 1 | INTRODUCTION

Around 1890, Emil von Behring and Shibasaburo Kitasato discovered a “specific antitoxic activity” in serum of animals infected with diphtheria. Nowadays, this activity can be attributed to proteins known as antibodies (Kenneth, Travors, & Walport, 2008). However, the concept of immunocytochemistry and its application in electron microscopy was developed much later. In the late 1950s, ferritin with a diameter of 11 nm was the first electron dense marker molecule that was coupled to antibodies (Singer & Schick, 1961). Without further treatment, only the iron-containing core of this molecule with a diameter of 5.5 nm is visible in the electron microscope. The so-called apo-ferritin shell can be visualized using alkaline bismuth solution (Ainsworth & Karnovsky, 1972). Up to now, a variety of marker molecules and enzymes for immunoelectron-microscopy is known, such as horseradish peroxidase

or iron dextrans (Dutton, Tokuyasu, & Singer, 1979; Nakane & Pierce, 1967). Being electron dense and manufacturable in uniform sizes, colloidal gold coupled to antibodies (immunoglobulin G proteins, IgGs) is preferably used in immunocytochemistry for electron microscopy (Faulk & Taylor, 1971; Slot & Geuze, 1985). Meanwhile, gold particles in various sizes down to 1 nm in diameter are commercially available. Via auto metallographic processes like silver enhancement, these nano-sized gold particles can be enlarged until the desired size is reached (Danscher, 1981; Stierhof, Hermann, Humbel, & Schwarz, 1995). Another instrument for antigen detection is protein A or G. These small molecules with a size of ~30–40 kDa exhibit a strong affinity to the F<sub>c</sub>-parts of antibodies from different species and can also be linked with gold particles (Romano & Romano, 1977; Roth, Bendayan, & Orci, 1978).

In particular, when performing immunocytochemistry experiments in electron microscopy not only the detection system is

This is an open access article under the terms of the Creative Commons Attribution License, which permits use, distribution and reproduction in any medium, provided the original work is properly cited.

© 2020 The Authors. *Microscopy Research and Technique* Published by Wiley Periodicals, Inc.

important for signal intensity and accuracy of localization, but also the sample preparation. The development of cryo preparation techniques (e.g., plunge freezing, propane jet freezing, high-pressure-freezing (HPF) and freeze substitution (FS)) significantly enhanced ultrastructural preservation of specimens, resulting in improved labeling efficiency of sensitive or of low copy number antigens (Humbel & Schwarz, 1989; Peschke, Moog, Klingl, Maier, & Hempel, 2013; Rachel et al., 2010). The use of cryo preparation methods aims at a near native preservation of cell structure. Ideally, the water content of the sample is vitrified after high-pressure freezing (Dahl & Staehelin, 1989; Moor & Riehle, 1968; Studer, Graber, Al-Amoudi, & Eggli, 2001). During freeze substitution the water in the sample is consecutively exchanged by organic solvents at  $-80$  to  $-90^{\circ}\text{C}$  to prevent formation of ice crystals (Steinbrecht & Müller, 1987). To stabilize cell structure, chemical fixatives like aldehydes, uranyl acetate or osmium tetroxide can be added to the substitution cocktail. Due to the fact that aldehydes are not reactive at temperatures below  $-40^{\circ}\text{C}$  (Humbel & Schwarz, 1989), the substitution solution can fully infuse the sample before aldehydes start to crosslink the specimen (Horowitz, Giannasca, & Woodcock, 1990). With regard to immunogold labeling, the use of osmium tetroxide being a strong oxidizing reagent and hence acting on epitope structure, is not recommended (Hopwood, 1969). Finally, samples are infiltrated with and embedded in resins, such as epoxy resins, which are recommended for ultrastructural investigations. Due to the strong cross-linking properties of epoxy resins, including reactions with the biological sample, antigenicity of the sample can be reduced (Stirling, 1990). This loss of antigenicity can be lowered when methacrylate resins like Lowicryl or London resins are used instead, because methacrylates can retain biochemical reactivity especially within partial dehydration. Furthermore, they offer more and sometimes more gentle polymerization possibilities like UV-polymerization at low temperatures (Newman & Hobot, 1999). In addition, Lowicryl resins do not co-polymerize with biological structures. Another fact that might lead to higher labeling efficiency on Lowicryl sections in comparison to epoxy resin sections might be the roughness of the section surface. Epon sections were found to be three times smoother than Lowicryl sections and therefore exhibiting less surface area, which also lowers the chance of accessible epitopes (Kellenberger, Dürrenberger, Villiger, Carlemalm, & Wurtz, 1987).

Although alternative ways of antigen (proteins, carbohydrates, etc.) localization for high-resolution microscopy are available (e.g., genetic tags coupled to fluorescent dyes for correlative microscopy), immunogold labeling is still a well-established and a widely applied technique for subcellular localization of antigens. Based on considerable experience in the field of antigen localization, we performed various experiments to unravel which of the circulating protocols for postembedding immunolabeling are still valid. In this article, we present our results on postembedding immunogold labeling on Epon sections in comparison to Lowicryl and Tokuyasu thawed cryo-section labeling. Furthermore, we freeze substituted samples of high-pressure frozen microorganisms with a cocktail containing significant amounts of osmium tetroxide. In addition, we developed an

accelerated protocol for protein localization and we compared labeling efficiency of secondary antibodies coupled to gold particles of different sizes. As a highlight, we present an alternative analytical method: three-dimensional immunogold labeling of serial ultrathin sections. Immunocytochemical investigations were performed on ultrathin sections of organisms we routinely grow and handle in our laboratories: *Ignicoccus hospitalis* (*I. hospitalis*), a hyperthermophilic prokaryote and *Phaeodactylum tricornutum* (*P. tricornutum*), a photosynthetic unicellular and eukaryotic microalga.

## 2 | MATERIALS AND METHODS

### 2.1 | Cultivation of organisms

*I. hospitalis* was cultivated anaerobically in modified  $\frac{1}{2}$  SME (i.e., half concentrated synthetic seawater medium; Paper et al., 2007). Serum bottles were inoculated in a dilution of 1:200 with a preparatory culture and incubated at  $90^{\circ}\text{C}$  while shaking (50 rpm).

*P. tricornutum* wild type was grown in f/2 medium and under constant illumination ( $80 \mu\text{mol photons} \times \text{m}^{-2} \times \text{s}^{-1}$ ) at  $22^{\circ}\text{C}$  as described previously (Hempel, Lau, Klingl, & Maier, 2011; Peschke et al., 2013). The cells were harvested via sedimentation for 1–2 hr and cryo-immobilized by high-pressure freezing as described below.

### 2.2 | Preparation of samples for electron microscopy

Cells of *Ignicoccus* were concentrated via filtration on top of a polycarbonate membrane with a pore size of  $0.2 \mu\text{m}$  using a syringe filter adapter. When working with *P. tricornutum*, cell density was increased via sedimentation for 1–2 hr.

For resin embedding, *Ignicoccus* and *Phaeodactylum* cells were immediately high-pressure frozen (EM PACT 2, Leica, Wetzlar, Germany; HPF compact 02, Wohlwend, Sennwald, Switzerland) to minimize the destructive contact to oxygen. This was followed by freeze substitution (AFS 2, Leica, Wetzlar, Germany) in acetone containing 0.5% (v/v) glutardialdehyde, 0.5% (w/v) uranyl acetate, and 5% (v/v) water, or in acetone containing 0.2% (w/v) osmium tetroxide, 0.1% (w/v) uranyl acetate and 9.3% (v/v) water, respectively. Then, cells were either embedded in the epoxy resin Epon 812 substitute resin (Fluka Chemie AG, Buchs, Switzerland), or in the methacrylate resin Lowicryl HM20 (Polysciences Inc., Warrington, FL). For freeze substitution and Epon embedding, we used the following protocol:  $-90^{\circ}\text{C}$  for 8 hr, heating to  $-60^{\circ}\text{C}$  within 6 hr,  $-60^{\circ}\text{C}$  for 8 hr, heating to  $-30^{\circ}\text{C}$  within 4 hr,  $-30^{\circ}\text{C}$  for 4 hr, heating to  $0^{\circ}\text{C}$  within 4 hr (*Ignicoccus*). The freeze substitution protocol for *P. tricornutum* differed slightly with a shorter heating step of 1 hr in between the respective temperature levels of  $-90$ ,  $-60$ , and  $-30^{\circ}\text{C}$ . Otherwise, the handling of *Phaeodactylum* was identical to *Ignicoccus*. Samples were then washed three times with ice cold acetone and infiltrated in acetone/Epon (2 + 1) for 1 hr at room temperature (RT,  $25^{\circ}\text{C}$ ),

acetone/Epon (2 + 1) for 1 hr acetone/Epon (1 + 1) for 2 hr, acetone/Epon (1 + 2) for 20 hr (all at RT) and in freshly prepared Epon for 2 hr at 30°C. Epon was polymerized at 60°C for 2 days (Rachel et al., 2010). For freeze substitution followed by Lowicryl-embedding, we used the following protocol: −90°C for 8 hr, heating to −60°C within 1 hr, −60°C for 6 hr, heating to −40°C within 1 hr, −40°C for 7 hr. After washing cells three times with acetone, cells were infiltrated with Lowicryl HM20 in acetone/Lowicryl (2 + 1) for 2 hr, acetone/Lowicryl (1 + 1) for 2 hr, acetone/Lowicryl (1 + 2) for 2 hr, and freshly prepared Lowicryl for 16 hr at −40°C. The polymerization of Lowicryl was performed under UV light at −40°C for 2.5 days.

Preparation of cryosections according to Tokuyasu based on protocols by George Posthuma, (Utrecht, the Netherlands) and was adapted accordingly for our samples (Möbius & Posthuma, 2018; Tokuyasu, 1973). Enriched samples were fixed in a PBS buffer (pH 7.2) containing 2% (v/v) formaldehyde and 0.1% (v/v) glutardialdehyde for 30 min at room temperature. To remove aldehydes, fixed samples were centrifuged at 6.000g for 15 min and washed with PBS buffer. After another centrifugation step, the resulting pellets were covered in a droplet of 10% gelatine, gently mixed and immediately transferred onto ice. After 15 min incubation on ice, gelatine-embedded cell pellets were cut into small cubes and infiltrated in 2.3 M sucrose overnight on a rotary incubator at 4°C. The following day, infiltrated blocks were mounted on aluminum pins and frozen in liquid nitrogen.

## 2.3 | Generation of antibodies

Antibodies directed against the *Ignicoccus* A<sub>1</sub>-part of the ATP synthase (polyclonal anti-A<sub>1</sub> antibodies were used in a dilution of 1:200), and antibodies directed against the acetyl-CoA synthetase (ACS; polyclonal anti-ACS antibodies were used in a dilution of 1:100) were raised in rabbits from the purified native complex (Heimerl et al., 2017; Küper, Meyer, Müller, Rachel, & Huber, 2010; Mayer et al., 2012). The monoclonal antibody against  $\beta$ -glucan chrysolaminarin was raised in mice and was purchased at Biosupplies (Australia).

## 2.4 | Immunogold labeling on resin sections

Immunogold labeling of ultrathin resin sections was performed according to the following protocol: Inactivation of free aldehyde groups in 1× PBS–glycine 0.1% (w/v) for 5 min, blocking in 1× PBS–BSA 1% (w/v) for 10 min, incubation with primary antibody diluted in 1× PBS–BSA 0.1% (w/v) for 15, 30, 60, or 90 min, five times washing in 1× PBS–BSA 0.1% (w/v) for 2 min, incubation with secondary antibody diluted in 1× PBS–BSA 0.1% (w/v) for 5, 15, 30, 60, or 90 min respectively, five times washing in 1× PBS–BSA 0.1% (w/v) for 2 min, two times washing in 1× PBS for 2 min, cross-linking of epitopes and antibodies in 1× PBS–glutardialdehyde 2% (v/v) for 5 min, two times washing in 1× PBS for 2 min, three times washing in H<sub>2</sub>O for 2 min. For detection of primary antibodies, goat anti-mouse or goat anti-rabbit secondary IgGs coupled to “ultrasmall”, 6, 10, and 15 nm gold

particles (Aurion, Wageningen, the Netherlands) were used. For secondary antibodies coupled to “ultrasmall” gold particles, immunolabeling was followed by silver enhancement using R-Gent SE-EM silver enhancement reagents (Aurion). Thereafter, sections were poststained with uranyl acetate 2% (w/v) in water.

## 2.5 | Immunogold labeling on Tokuyasu sections

Immunogold labeling of thawed cryosections was performed as described previously with slight variations (Tokuyasu, 1973; Griffiths, McDowall, Back, & Dubochet, 1984; Möbius & Posthuma 2018; Webster & Webster, 2014): three times washing in 1× PBS for 2 min, inactivation of free aldehyde groups in 1× PBS–glycine 0.1% (w/v) for 15 min, blocking in 1× PBS–BSA 1% (w/v) for 30 min, incubation with primary antibody diluted in 1× PBS–BSA 0.1% (w/v) for 45 min, five times washing in 1× PBS–BSA 0.1% (w/v) for 2 min, incubation with secondary antibody diluted in 1× PBS–BSA 0.1% (w/v) for 45 min, five times washing in 1× PBS–BSA 0.1% (w/v) for 2 min, two times washing in 1× PBS for 2 min, cross-linking of epitopes and antibodies in 1× PBS–glutardialdehyde 2% (v/v) for 5 min, two times washing in 1× PBS for 2 min, three times washing in H<sub>2</sub>O for 2 min. For detection of primary antibodies, goat anti-rabbit secondary IgGs coupled to “ultrasmall” or 6 nm gold particles (Aurion) were used. For secondary antibodies coupled to “ultrasmall” gold particles, immunolabeling was followed by silver enhancement using R-Gent SE-EM silver enhancement reagents (Aurion). Thereafter, sections were poststained with 2% uranyl oxalate/acetate, pH 7 (Griffiths et al., 1984; Möbius & Posthuma, 2018) for 5 min and with uranyl acetate 0.4% (w/v) in 2% methylcellulose (w/v) for 5 min on ice. Afterward, sections were embedded in a thin layer of uranyl acetate 0.4% (w/v) in 2% methylcellulose. For this, a drop containing the solution was applied on parafilm. Grids were then fished with a wire loop and were dried with a filter paper. Grids were allowed to further dry in the loop for 30 min. Finally, they were carefully removed from the loop with a syringe or with tweezers.

## 2.6 | Transmission electron microscopy

Transmission electron microscopy was mainly performed on a 120 kV Philips CM12 (Thermo Fisher Scientific) equipped with a LaB<sub>6</sub> cathode and a 1 k × 1 k slow-scan CCD camera and EM Menu 4.0 (TVIPS, Gauting, Germany). Additionally, we used a Zeiss EM 912 with an integrated OMEGA-filter with an acceleration voltage of 80 kV which uses a 2 k × 2 k slow-scan CCD camera with the respective software package (Tröndle Restlichtverstärker Systeme, Moorenweis, Germany).

## 2.7 | Image processing and three-dimensional (3D) reconstruction

Image- and data processing was performed using Image J (Schneider et al., 2012), Photoshop CS5 and Adobe Illustrator (Adobe, San Jose,

CA). For 3D reconstructions, we used serial ultrathin sections with a nominal thickness of 70 nm. Segmentation and 3D reconstruction of EM data was carried out with AMIRA (Thermo Fisher Scientific) as described previously (Heimerl et al., 2017).

### 3 | RESULTS

#### 3.1 | Immunolabeling on Epon sections versus Lowicryl- and Tokuyasu sections

It is generally accepted that epoxy section labeling is less effective than comparable experiments on Lowicryl- or cryosections. However, recognizability of ultrastructural details of epoxy resin embedded cells was excellent and even superior to cells embedded in methacrylate resins or cells prepared for Tokuyasu cryosection labeling. The better structural preservation was caused by the respective fixation technique that was applied but also by the resin itself. At this point it should be mentioned that the visibility of membranes is usually excellent in Tokuyasu cryosections but the silver enhancement might have had a negative effect on the bilayer delineation. In the course of this study, high-pressure-frozen cells of the hyperthermophilic archaeon *I. hospitalis* were freeze-substituted without osmium tetroxide. Cells were then embedded in two different resins (Epon 812 substitute medium and Lowicryl HM20), and cryosections were prepared according to Tokuyasu. We compared the structural preservation of the cells and the relative labeling intensity after immunocytochemical treatment. Table 1 summarizes primary antibodies (incubated for 60 min) tested on ultrathin sections of *I. hospitalis* and their binding behavior on different resins or on cryosections, respectively. Three (antibodies directed against DNA, against phosphoenolpyruvate carboxylase and against malate dehydrogenase) out of six of the tested antibodies, did not bind to Epon sections at all, but did, however, to Lowicryl- and/or to cryosections (Table 1). Labeling of Lowicryl- or of Tokuyasu sections (even with higher dilutions of primary antibodies) led to high signal intensities for the same antibodies. Figure 1 illustrates immunogold staining on Epon- (a and d), on Lowicryl- (b and e) and on Tokuyasu sections (c and f). Here, we located the archaeal  $A_1$ - $A_0$  ATP synthase, an enzyme involved in the energy metabolism of the archaeon *I. hospitalis*. The background signal on each section was

low, indicating the specificity of the antibodies. Comparing the density of gold particles, Lowicryl- and cryosection labeling indeed appeared to be more sensitive than epoxy resin labeling. To avoid unspecific labeling, lower concentrations of primary and secondary antibody were applied on cryosections, which show the highest label density. However, Epon sections (Figure 1a,d,g,i) impressed apparently by their excellent preservation of details, resulting in a clearly visible compartmentalized cell structure and an electron dense cytoplasm. Especially the filamentous structures in the intermembrane compartment (IMC) were clearly delineated on Epon resin sections, and the lipid bilayer of the cytoplasmic membrane was visible. Preservation of Lowicryl-embedded cells was sufficient but to some degree compromised (Figure 1b): the compartmentalized character of the cell was still recognizable, but with fewer details. Moreover, no bilayer could be depicted and cytoplasmic protrusions and vesicles appear blurrier. Occasionally, we observed cells that were totally or half broken out of the resin. Cell preservation on cryosections was very heterogeneous and varied from sufficient to poor (Figure 1c,f,h,j). Partially, we observed well-preserved cryo-sectioned cells with visible membranes (Figure 1f,h; Flechsler, 2015). At this point it should be mentioned, that silver enhancement often interferes with structural preservation and therefore might have led to the differences in Figure 1c,h.

In conclusion, all three methods led to very similar labeling patterns although ultrastructural preservation of cells was diverse. Additionally, we showed that labeling on Epon sections, if possible, was a good alternative to localization on Lowicryl sections and on Tokuyasu cryosections, with the benefit that precise subcellular localization coincided with good ultrastructure (Flechsler, 2015; Griffith, Mari, De Mazière, & Reggiori, 2008).

#### 3.2 | Immunolabeling of sections containing osmium

To illustrate the efficiency of immunostaining on sections containing significant amounts of osmium tetroxide ( $OsO_4$ ), we used *P. tricornutum* cells, which were high-pressure frozen, freeze substituted with a solution containing 0.2% of  $OsO_4$ , and embedded in Epon 812 substitute resin. Figure 2 shows a *P. tricornutum* cell immunolabeled with an antibody against the  $\beta$ -glucan chrysolaminarin, a linear polymer of  $\beta(1$

**TABLE 1** Binding behavior of antibodies on ultrathin sections of *Ignicoccus hospitalis* prepared in three different ways

Antibody	Epon	Lowicryl	Tokuyasu
$\alpha$ -DNA	—	+	++
$\alpha$ - $A_1$ - $A_0$ ATP synthase	+	++	++
$\alpha$ -PEP carboxylase	—	+	++
$\alpha$ -malate dehydrogenase	—	+	++
$\alpha$ -succinic semialdehyde reductase	+	no data	++
$\alpha$ -crotonyl-CoA hydratase/3-hydroxybutyryl-CoA dehydrogenase	+	++	++

Note: Signal intensity: — no signal, + good signal, ++ strong signal. Based on Flechsler, 2015.



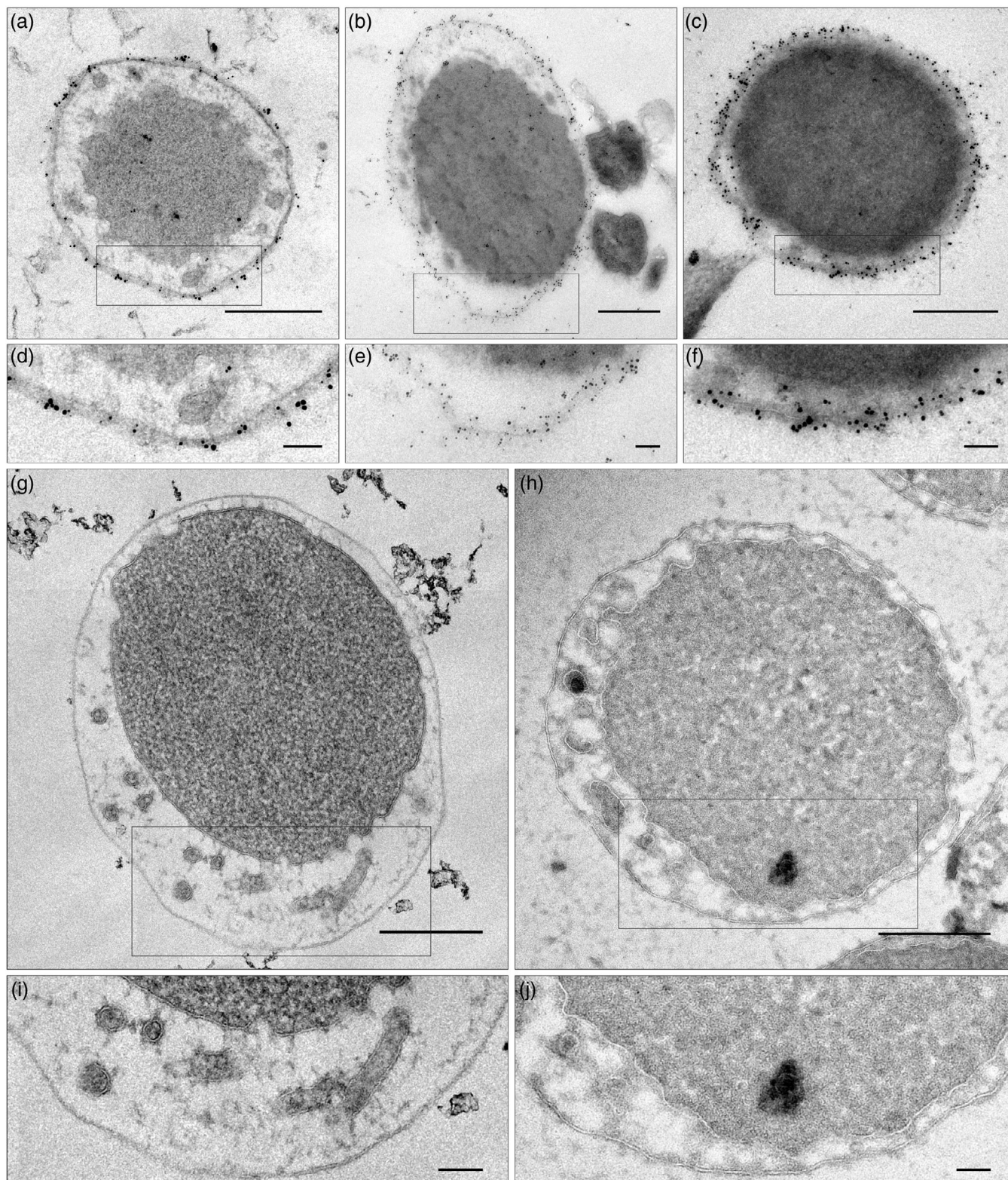


**FIGURE 1** Comparison of immunolabeling on Epon-, on Lowicryl- and on cryosections. Epon section (a and d, 1° AB 1:200, 2° AB 1:50), Lowicryl section (b and e, 1° AB 1:200, 2° AB 1:50), cryosection (c and f, 1° AB 1:500, 2° AB 1:100) of *Ignicoccus hospitalis* cells labeled with an antibody directed against archaeal A<sub>1</sub>-A<sub>O</sub> ATP synthase. Silver enhancement of the ultrasmall gold particles for 35 min. g–j: Unlabeled Epon- (g,i) and unlabeled cryosection (h,j) of *I. hospitalis*. Modified from Flechsler (2015). Scale bars: 500 nm (a–c, g, h), 100 nm (d–f (zoom-ins on a–c), i, j (zoom-ins on g, h))



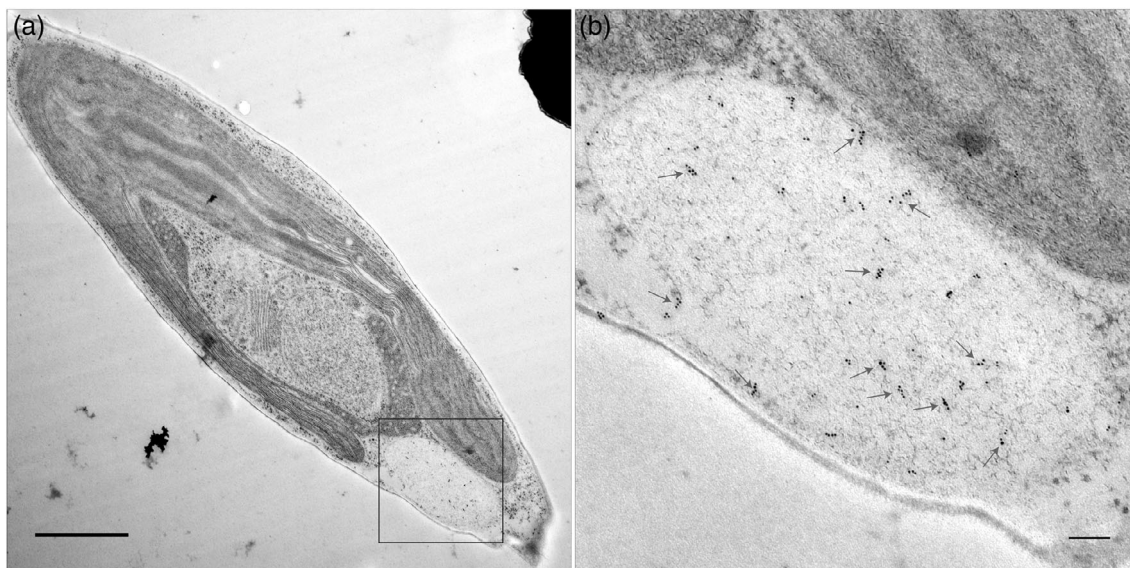


**FIGURE 2** Immunolabeling on ultrathin sections of Epon-embedded *Phaeodactylum tricornutum* cells (0.2% OsO<sub>4</sub> during freeze substitution). 1° AB: anti- $\beta$ -glucan diluted 1:10,000; 2° AB: 6 nm gold diluted 1:50. b: Higher magnification of the marbled vacuole. Arrows indicate gold particles in the vacuole. Scale bars: 500 nm (a), 100 nm (b)

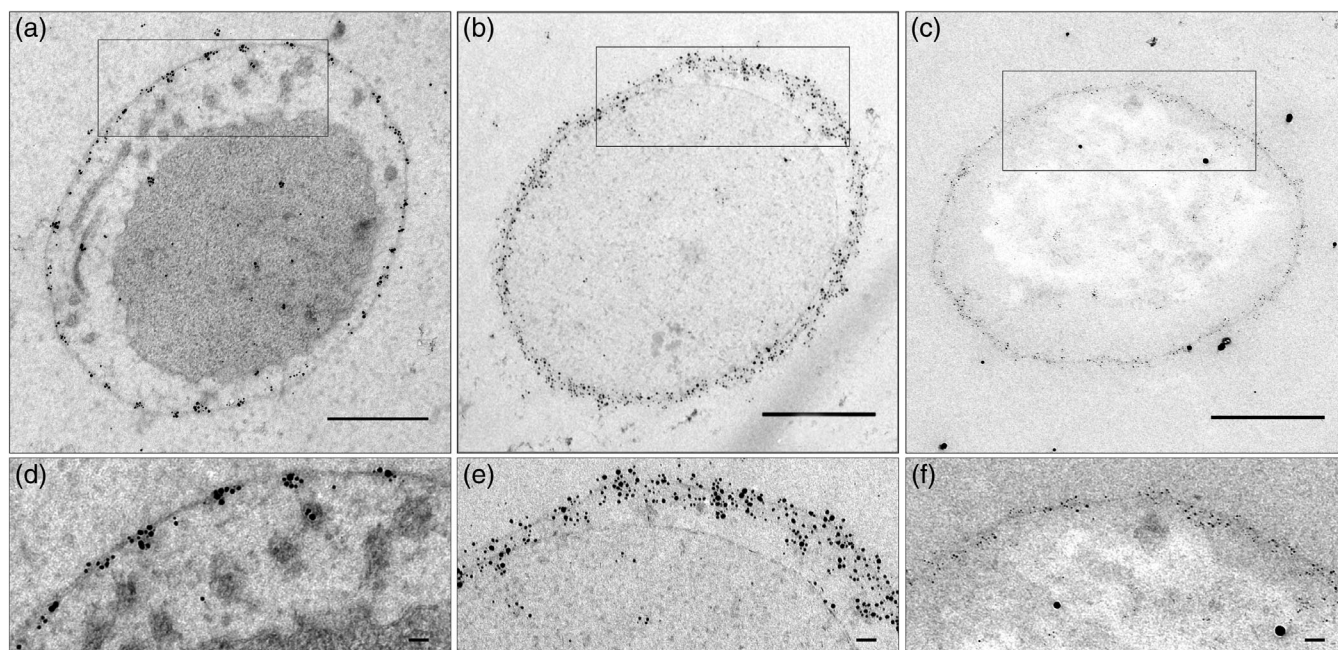


**FIGURE 3** Speed immunolabeling on ultrathin sections of Epon-embedded *Ignicoccus hospitalis* cells depicting the structural preservation. 1° AB: anti-ACS diluted 1:100; 2° AB: ultrasmall gold diluted 1:50; Gold particles were enlarged with a silver-enhancement solution for 25 min; a: Incubation time of 1° and 2° AB 30 min. b: Incubation time of 1° and 2° AB 60 min. c: Incubation time of 1° and 2° AB 90 min. Modified from Flechsler (2015). Scale bars: 500 nm (a–c), 50 nm (d–f (zoom-ins on a–c))

– > 3) and  $\beta(1 \rightarrow 6)$  linked glucose units, which is also known as leucosin. As documented in previous studies, the antibody exclusively localized to the vacuole of the microalgae (Schreiber et al., 2017). At this point, the excellent overall structural preservation has to be noted. The complex plastid showed a clear delineation of the thylakoid membranes and the dot-like internal membranes of the mitochondrion were visible

as was the Golgi stack. Also the content of the vacuole was visible (marbled vacuole). In comparison to this, chemically fixed cells, dehydrated in a graded ethanol or acetone series at RT, could not be used for the localization of chrysolaminarin. The reason for this might be the complete loss of vacuolar content within the fixation and dehydration procedure, the loss of antigenicity or a combination of both.



### 3.3 | Speed immunolabeling

In commonly used protocols for immunogold labeling on ultrathin sections, antibody incubation steps are usually carried out for one or two hours. After the complete procedure, which generally takes 4 to 5 hr, we frequently observed immunolabeled cells that showed reduced contrast and visibility of structural details (Figure 3b,c) compared to nonlabeled cells or to cells with shorter incubation times (Figure 3a). Therefore, an experiment was performed in which both antibody incubation steps were gradually shortened. Immunolabeled Epon sections of *I. hospitalis* cells, incubated with primary (A<sub>1</sub> part of the archaeal ATP synthase) and secondary antibodies for 5, 15, 30, 60 and 90 min, respectively were compared regarding labeling density and structural preservation. Figure 4 shows immunolabeled cells incubated with primary and secondary antibodies for 5–30 min, respectively (Figure 4a–c). The zoom-ins Figure 4d–f) on the sections labeled for the respective incubation times give a more detailed view on the gold particles distributed along the outer cellular membrane (OCM). According to these results it became clear that gold particle density increases with time (5–90 min; Figures 3 and 4). However, our study also suggests, that labeling density is absolutely sufficient after 30 min incubation time at least when using antibodies linked to 1 nm gold particles. We want to highlight that even antibody incubation times of 5 and 15 min resulted in a specific labeling pattern with a significant number of gold particles in the *I. hospitalis* OCM (Flechsler, 2015; Küper et al., 2010). Furthermore, we observed 5 to 10% of gold particles in the cytoplasm of *I. hospitalis*. According to previous studies, these labels could be considered as specific since the enzymes are most probably synthesized in that compartment and transported to the OCM (Küper et al.,

2010; Mayer et al., 2012). Regarding structural preservation of details, the accelerated protocol scored considerably better. Figure 3 shows an immunolocalization of the ACS on ultrathin sections of *I. hospitalis* incubated with antibodies for 30 (Figure 3a), 60 (Figure 3b) and 90 min (Figure 3c). Already at the first glance, the cell with the shortest total incubation time (Figure 3a) revealed the most structural details. In Figure 3a,b, the OCM, the IMC, and the cytoplasm could be distinguished, taking into account that the cytoplasm of the cell in Figure 3c was bleached. However, in Figure 3a, the OCM, the IMC, and the cytoplasm can clearly be recognized, and additionally cytoplasmic protrusions in the IMC are visible. Thus, we concluded that incubation times of 30 min for primary and secondary antibody each can be absolutely sufficient to obtain specific labeling patterns and can even lead to better visibility of ultrastructural details (Flechsler, 2015).

### 3.4 | Influence of gold particle size on efficiency of immunolabeling

Not only good quality of primary antibodies and the preservation of fine structure, but also the gold particle size had a decisive impact on the results of immunocytochemistry experiments. To clearly depict the effect of the gold particle size on labeling intensity, we immunostained cells of *I. hospitalis* with primary antibodies directed against the archaeal ATP synthase and secondary antibodies coupled to gold particles of different sizes, namely “ultrasmall-”, 6, 10, and 15 nm gold particles (Figure 5). Comparing cells labeled with gold particles of different sizes, it became obvious that the highest labeling intensity was

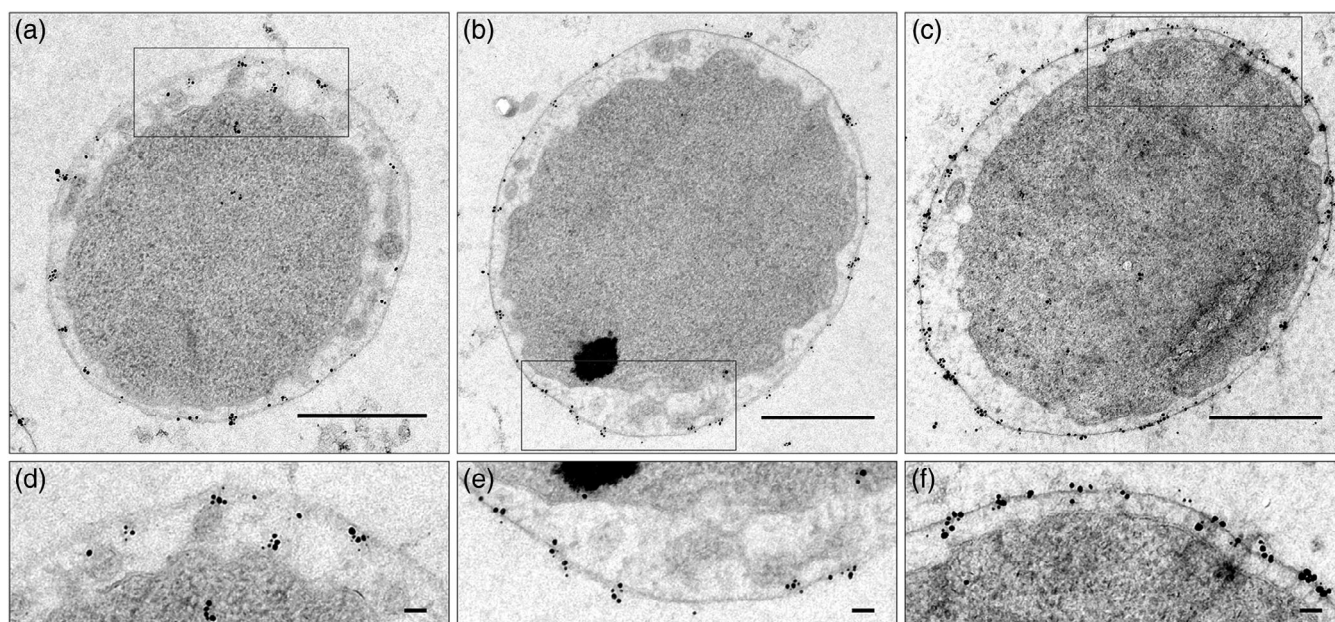


**FIGURE 4** Speed immunolabeling on ultrathin sections of Epon-embedded *Ignicoccus hospitalis* cells regarding signal intensity. 1° AB: anti-A<sub>1</sub> diluted 1:200; 2° AB: ultrasmall gold diluted 1:50; Gold particles were enlarged with a silver-enhancement solution for 25 min; a and d: Incubation time of 1° and 2° AB 5 min. b and e: Incubation time of 1° and 2° AB 15 min. c and f: Incubation time of 1° and 2° AB 30 min. d, e, and f: zoom-in on gold particles in the OCM. Modified from Flechsler (2015). Scale bars: 500 nm (a–c), 50 nm (d–f)



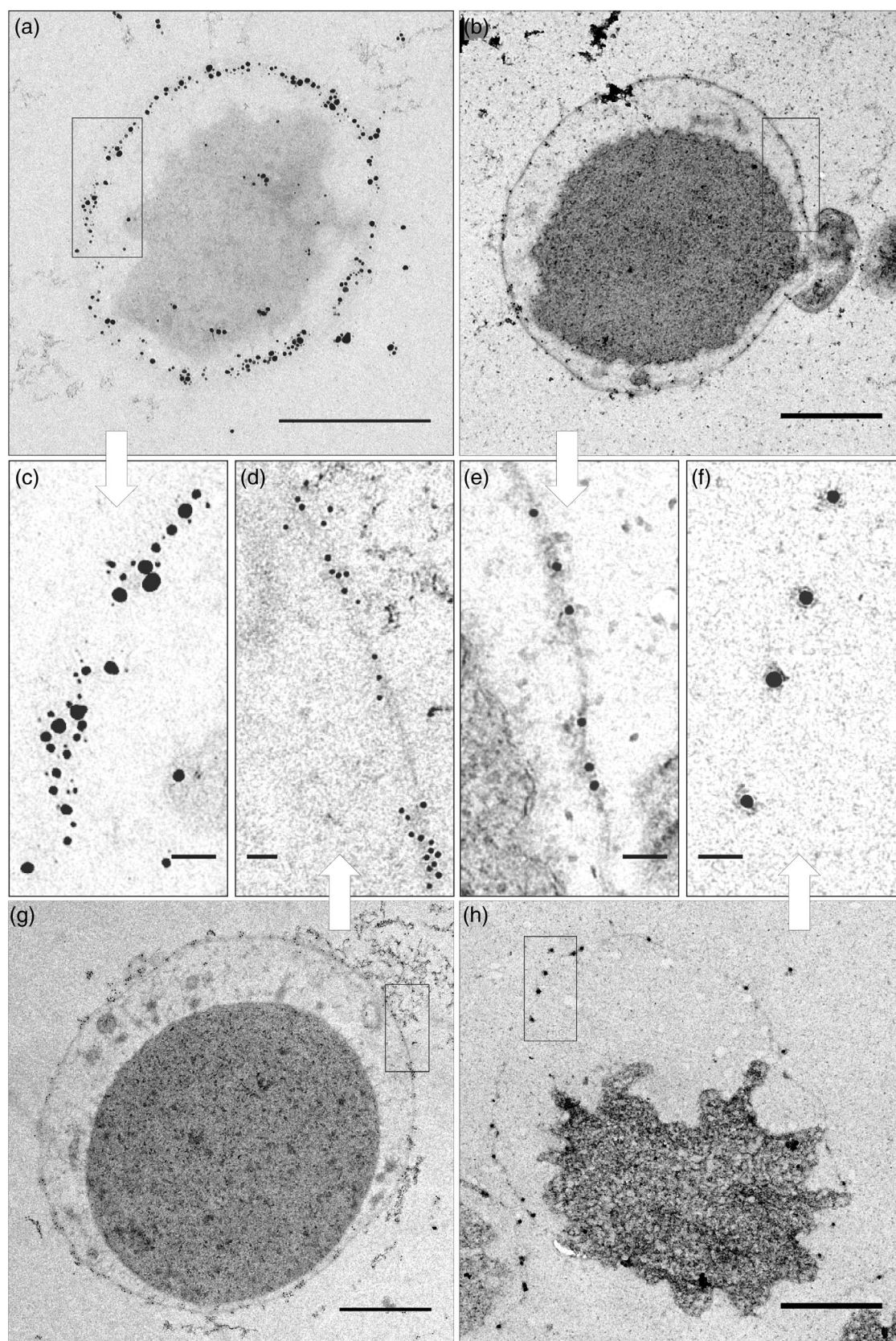


**FIGURE 5** Comparison of four different secondary ABs coupled to gold particles of different sizes. *Ignicoccus hospitalis* cells were labeled with a 1° AB directed against the archaeal  $A_1$ - $A_O$  ATP synthase (diluted 1:200) and with different 2° ABs (ultrasmall-gold + silver enhancement (a,c); with 6 nm-gold (g,d), with 10 nm-gold (b,e), and with 15 nm-gold (h,f). 2° ABs were diluted 1:50. Scale bars: 500 nm (a,b,g,h), 50 nm (c-f)



achieved using “ultrasmall” gold particles (Figure 5a). As described previously, we observed a decreasing binding intensity by increasing size of gold particles from ultrasmall gold (Figure 5a,c) to 15 nm gold particles (Figure 5f,h; Gu & D'Andrea, 1989). Supporting Information S1 shows a model representation of immunogold-labeled ultrathin sections with secondary antibodies that are coupled to differently sized gold particles with antibodies and gold particles drawn in scale. The model emphasizes the steric hindrance that arises from and increases with the gold particle size.

### 3.5 | 3D immunogold labeling

Beside localization of protein and carbohydrate epitopes in two dimensional (2D), 3D data sets were collected using serial ultrathin sections

to investigate the spatial distribution of gold particles and antigens, respectively. On the basis of serial sections followed by subsequent immunolabeling, images were recorded for the generation of 3D models (also see Flechsler, 2015). Supporting Information S2 shows 16 selected images from a series of 20 images in total of an *I. hospitalis* cell connected with one cell of *Nanoarchaeum equitans* (*N. equitans*), which is a prokaryotic organism that lives in direct association with *I. hospitalis*. The images were collected from serial sections of Epon-embedded cells à 70 nm and cells were immunolabeled with an antibody directed against the ACS. The overall good ultrastructural preservation is particularly striking in this case. In 2D, the majority of gold particles were evenly distributed following the curvature of the OCM. Only few labels could be detected in the cytoplasm and almost no gold particles could be found in the background. Figure 6a–e shows the 3D reconstruction of the data set (Supporting Information S2–Supporting Information S4).

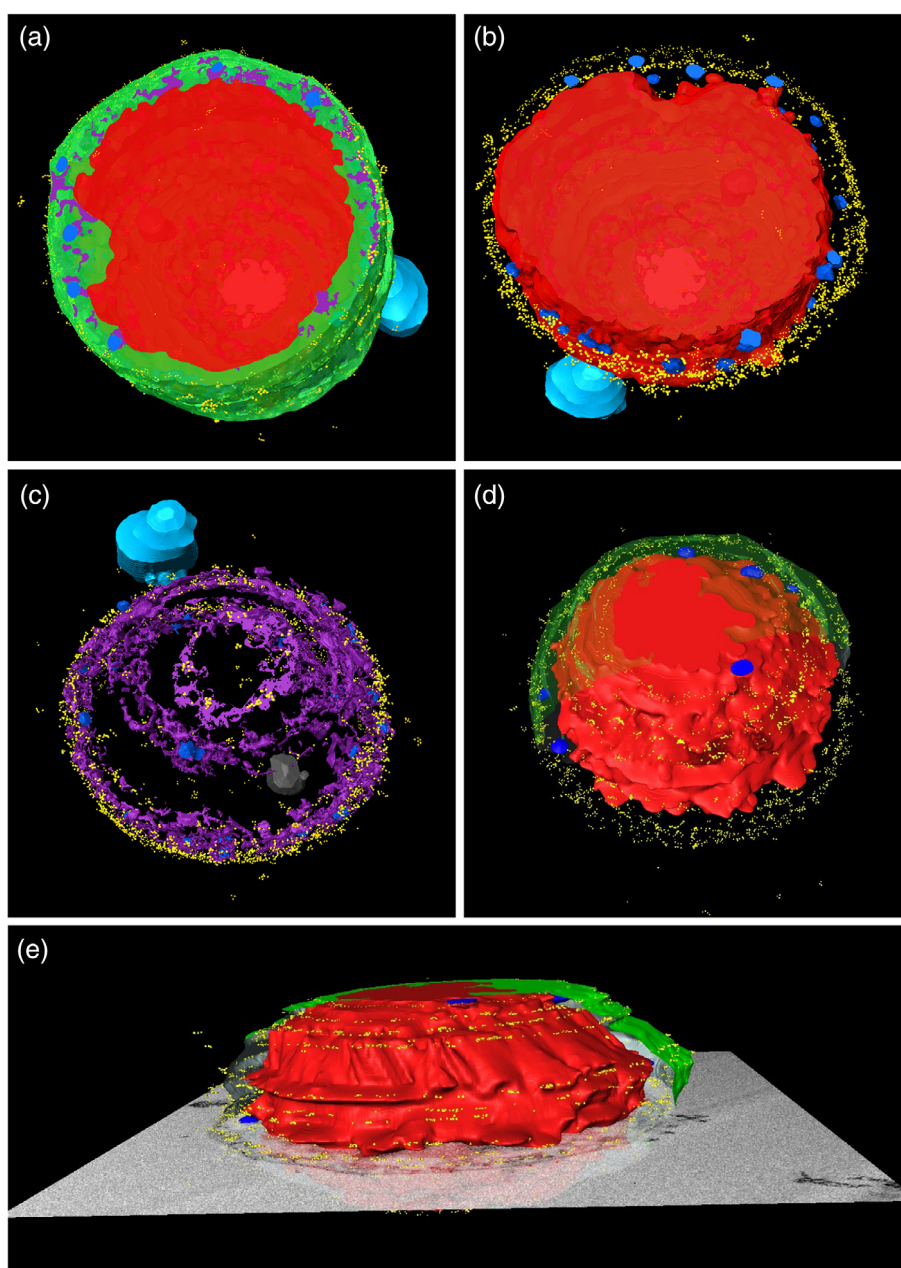


**FIGURE 6** 3D-reconstruction and visualization of a data set of serial sections from *Ignicoccus hospitalis* from various orientations. In the subpanels, selected cell components like the IMC are highlighted (a) or left out (b,d), especially for better visibility of internal structures in the cytoplasm or the intermembrane compartment (IMC) (c). e: 3D-reconstruction of serial sections with one of the referring sections included at the bottom. Cells were prepared as described and labeled with a 1° AB directed against the ACS and detected with 2° AB: 6 nm gold diluted 1:50. Red: Cytoplasm and inner membrane (IM); green: IMC and outermost cellular membrane (OCM); yellow: gold particles; dark blue: vesicles; purple: structures in the IMC; dark grey: putative phosphate storage; light blue: one cell of *Nanoarchaeum equitans* linked with *I. hospitalis*. Majority of gold particles is located in association with the OCM, only few are located in the cytoplasm. Based on Flechsler (2015)

Figure 6a and d displays the bottom and the top view on the reconstruction including all observed structures and compartments. The cytoplasm is colored in red, whereas OCM and IMC are green. Gold particles are shown as yellow dots and putative vesicles are dark blue. *N. equitans* is shown in light blue. Furthermore, the structure labeled in purple represents a previously unknown structure in the IMC, which has been described recently as filamentous matrix (Heimerl et al., 2017). These filamentous structures in the IMC are suspected to be involved dynamic processes of the endogenous membrane system (Heimerl et al., 2017). Figure 6e shows the reconstruction from a side view with an original micrograph.

In this side view, gold particles appear in rings around the cytoplasm in fixed intervals. The distance of the individual rings is due to serial sections of 70 nm, since antibodies cannot penetrate the sections, and thus, only bind to their surface. Similarly to the localization in 2D, gold particles in 3D-models could be found preferably in the OCM, underlining the high specificity of this immunocytochemistry experiment. In almost every section, few gold particles were found in the cytoplasm.

## 4 | DISCUSSION

### 4.1 | Immunolabeling on Epon sections versus Lowicryl sections and Tokuyasu cryosections

In this study, efficiency of immunogold labeling and preservation of ultrastructure of samples was compared on Tokuyasu cryosections and on resin sections (Epon vs. Lowicryl). With an often two- to three-fold enhanced labeling intensity Tokuyasu cryosection labeling is considered the “most efficient procedure for immunogold labeling” (Kellenberger et al., 1987; Peters, Bos, & Griekspoor, 2006). Advantages of the Tokuyasu method are that aldehyde fixation is the only potential denaturation step and antigens are kept in an aqueous medium for the whole procedure. Therefore, the loss of antigenicity is not caused by harsh organic solvents during dehydration and embedding (Griffiths, 1993; Schwarz & Hohenberg, 2001). In addition, the accessibility of antigens is enhanced compared to resin embedded antigens (Stierhof & Schwarz, 1989). For immunocytochemistry on resin sections, the majority of electron microscopists generally prefer embedding in methacrylates. The higher roughness of the surface of methacrylate sections compared to epoxy sections (three times rougher than that of epoxy sections (Kellenberger et al., 1987)) might contribute to the often higher label density. Maybe even more importantly, and in contrast to methacrylates, epoxy resin components also react with biological molecules. In addition, Lowicryl resins infiltrate and polymerize (under UV) at temperatures below  $-30^{\circ}\text{C}$ , which is below the so-called collapse temperature. At these temperatures, structural bound water, which contributes to the integrity of molecules and thus to their near natural preservation, is not removed completely. Lowicryl resins can deal with elevated amounts of water (Hobot, 1990) and this characteristic is also advantageous for freeze substitution with solutions containing small amounts of water.

Dehydration approaches like progressive lowering of temperature (PLT) and also freeze substitution following high-pressure freezing are therefore assumed to be less harmful to cells and tissues than dehydration at ambient temperatures and polymerization of Epon or Araldite resins at 60 up to  $100^{\circ}\text{C}$  (Hobot, 1990; McDonald, 2014; Shiurba, 2001). All these facts indicate a decreased antigenicity of biomolecules in Epon-embedded samples, and/or a highly reduced accessibility of the antibodies to the targets. Therefore, Epon appears to be and is often quoted as an inappropriate embedding resin for immunogold localization in electron microscopy (e.g., “a drawback of the “HPF-freeze substitution-Epon” embedding method is that most molecules lose their antigenicity during the procedure” in Zeuschner et al., 2006). Nevertheless, there are a number of examples for successful labeling of epoxy resins after conventional processing or cryofixation/freeze-substitution. These include small neurotransmitter labeling (Ottersen, Zhang, & Walberg, 1992), immunolabeling, and lectin labeling of carbohydrate epitopes (Moussian et al., 2006; Ndinyanka Fabrice et al., 2017; Richter et al., 2012), immunolabeling of proteins (Groos, Reale, & Luciano, 2001), biotin of biotinylated proteins (Viens et al., 2008), glycoinositolphospholipids, and glycosphingolipids (Winter, Fuchs, McConville, Stierhof, & Overath, 1994). The experiments shown in this study, but also in previous studies from our laboratory demonstrated that Epon sections can be superior for many immunolabeling studies, at least when studying archaeal cells and microalgal cells (Heimerl et al., 2017; Küper et al., 2010; Liu et al., 2016; Mayer et al., 2012; Meyer, Heimerl, Wirth, Klingl, & Rachel, 2014; Mix et al., 2018; Peschke et al., 2013; Schreiber et al., 2017). Slight changes in the chemical nature of nowadays resins compared to the 1970s and 1980s (e.g., Embed 812 from Electron Microscopy Sciences as replacement product for EPON 812; Luft, 1961) make epoxy resins a lot more useful than generally thought (Frankl, Mari, & Reggiori, 2015; Stirling, 1990). However, it needs to be noted that we were not able to detect gold particles on Epon sections with three out of six tested primary antibodies (Table 1). These antigens could in contrast be detected on Lowicryl- and on Tokuyasu-sections with strong signal intensities. For all other tested antibodies, a strong signal was present on sections of Epon- and of Lowicryl-embedded *Ignicoccus* cells, and on cryosections prepared according to Tokuyasu. In our study, the Tokuyasu technique indeed turned out to be the most sensitive method for immunocytochemistry. Signal intensity on Tokuyasu sections was increased compared to that on Lowicryl sections, and was higher than labeling on Epon sections, although higher dilutions of antibodies were used in Tokuyasu experiments. However, using epoxy resins turned out to be the method of choice when focusing on ultrastructural preservation in combination with immunocytochemistry. For *Ignicoccus*, an excellent cellular ultrastructure was obtained throughout using Epon as embedding resin, provided that it was preceded by gentle cell harvesting, HPF and an appropriate, optimized freeze substitution protocol. On the contrary, we occasionally observed cells that were broken out of the resin when embedded in Lowicryl. This might be due to Lowicryl not reacting covalently with the sample (Griffiths, 1993). Preservation of cells prepared according to Tokuyasu was extremely variable and ranged from good to poor,



which might be due to silver enhancement or gelatin embedding of the sensitive cells or due to material extraction after thawing the sections (Flechler, 2015; Liou, Geuze, & Slot, 1996).

Finally, immunocytochemistry experiments using three different preparation methods led to similar results. This demonstrated the meaningfulness of immuno-EM in this study. Although resulting in lower labeling efficiency, a striking advantage of Epon sections is their excellent structural visualization capability, which enables or facilitates the identification of labeled structural details on an ultrastructural level. Thus, we conclude that Epon sections can be considered as a good alternative to methacrylate and thawed cryosections if antigens are still detectable. Lowicryl and thawed cryosections can be used as additional controls for labeling experiments.

## 4.2 | Immunogold labeling of sections containing OsO<sub>4</sub>

The application of OsO<sub>4</sub> as postfixation and staining agent in electron microscopy has some clear and obvious advantages. The improved fixation and retention of lipids in membranes and of other components containing C–C-double bonds leads to a significant better structural preservation. That is extremely important, when the presence of certain membranes and their shape and positioning is necessary for the scientific output of the investigation. A good preservation of bilayers can be accomplished by the application of the Tokuyasu technique, by low concentrations of tannic acid (Berryman, Porter, Rodewald, & Hubbard, 1992), the application of uranyl acetate alone as postfixative or by the addition of OsO<sub>4</sub>. Using uranyl acetate for postfixation in immunocytochemical studies led to an enhancement of membrane ultrastructure without apparent effects on the respective antigens in these experiments (Berryman & Rodewald, 1990; Valentino, Crumrine, & Reichardt, 1985). An example for the application of OsO<sub>4</sub> was the visibility of the complex plastid membranes in diatoms such as *P. tricornutum* (Peschke et al., 2013; Schreiber et al., 2017). Other cell structures that benefit from the use of OsO<sub>4</sub> are mitochondria, the nucleus with the nuclear envelope, the Golgi apparatus and the endoplasmic reticulum. However, OsO<sub>4</sub> reduces the antigenicity of desired localization targets and negatively influences the accessibility of epitopes. Furthermore it was shown, that higher concentrations of OsO<sub>4</sub> could have a cell component destructive, proteolytic, and actin filament degrading effect (Baschong et al., 1984; Behrman, 1984; Locke, 1994; Maupin & Pollard, 1983; Maupin-Szamier & Pollard, 1978). Therefore, and if it cannot be avoided as supposed by Hopwood (1969) and others (Frankl et al., 2015), a reduction of the OsO<sub>4</sub> concentration makes sense. However, the application of OsO<sub>4</sub>-concentrations in the range of 0.2 or 0.3% instead of 2% in freeze substitution significantly reduces the negative effect of the chemical but still enables very good structural details (Liu et al., 2016; Maupin & Pollard, 1983; Mix et al., 2018; Peschke et al., 2013). Depending on the sample, even a reduction to 0.02% OsO<sub>4</sub> delivered satisfying structural preservation (data not shown). In addition, the reduced dark OsO<sub>4</sub> staining resulted in less interference with the polymerization by UV light in the case of Lowicryl sections. In our

experience, cryo-fixation via high-pressure freezing prior to the application of OsO<sub>4</sub> in freeze substitution was a prerequisite for successful immunogold localization as the close-to-natural preservation in this freezing technique prevents damage of epitopes and therefore diminished the negative effects of OsO<sub>4</sub>. In addition, we were using epoxy resins (usually Epon 812 substitute resin) as embedding media for immunogold labeling because of the improved ultrastructure compared to methacrylate resins.

Finally, it should be mentioned, that there have also been studies performing postembedding immunogold electron microscopy of chemically fixed biological material with low concentrations of osmium tetroxide (0.1% OsO<sub>4</sub>; Lehtreck, Teltenkötter, & Grunow, 1999; Pedersen, Geimer, & Rosenbaum, 2006).

## 4.3 | Speed immunolabeling

In protocols for postembedding labeling, incubation times for primary antibodies range from 30 min (Aurion's protocol for immunogold labeling) to 18 hr (Miyake & Colquhoun, 2012). Similar referrals, varying from 45 min to 2 hr (Richards, Owen, Riehle, Gwynn, & Curtis, 2001) were found for secondary antibodies. However, according to Griffiths, high affinity binding can be observed more quickly than non-specific binding and incubation of 5 to 30 min suffices (Griffiths, 1993). Additionally, the group of Hyatt reported that specific labeling could be achieved after 15 min incubation of both, primary and secondary antibody (Hyatt, 1991). To find out the best parameters for labeling of *Ignicoccus* proteins, different incubation times of primary and secondary antibodies were compared regarding labeling density and structural preservation of cells. In the following, the term "incubation time" is used in a generalized sense and refers to both, primary and secondary antibody incubation steps. In this experiment, two primary antibodies were used whose binding behavior on cells of *I. hospitalis* have been studied for a while in our laboratory (anti-A<sub>1</sub>-A<sub>O</sub> ATP synthetase and anti-ACS). This resulted in specific labeling of the *Ignicoccus* OCM after incubation of sections for 5 and 15 min using the anti-A<sub>1</sub>-A<sub>O</sub> ATP synthetase antibody. After 30 min incubation, a significant amount of gold particles was observed on ultrathin sections that specifically bound to the *Ignicoccus* OCM (Flechler, 2015) with comparable results to longer incubation times (Küper et al., 2010).

However, there was no substantial difference regarding signal intensity after 60 min and after 90 min incubation time, respectively. These observations were in line with reports by Hyatt who showed that immunogold labeling reaches a saturation level after 60 min incubation at room temperature, or at 37°C (Hyatt, 1991). Griffiths performed similar studies to this approach on thawed cryosections, using two different antibodies. In this experiment, two different incubation times were tested, namely, 30 min and 3 hr, and in addition concentration of antibodies were varied. The results of this study suggested that incubation times longer than 30 min have only limited impact on the signal (Griffiths, 1993). Apparently, in our study preservation of the ultrastructure appeared to be different depending on the incubation times. Long incubation steps (90 min) frequently led to bleached

cells, as shown in an extreme example in Figure 3a. This finding was similar to a previous study of Berryman and Rodewald (1990). In general, cells were well preserved after a 30 min incubation period. The use of an accelerated protocol clearly demonstrated that shorter incubation times (30 min) may often suffice for immunolabeling and contribute to better preservation of ultrastructural details. With respect to cells of *Ignicoccus*, a detailed preservation of ultrastructure was of major importance regarding labeling of fine structures in the IMC. Also the ultrastructural preservation of eukaryotic samples might benefit from shorter incubation times of immunolabeling experiments. However, one should bear in mind that optimal incubation times and additional parameters (e.g., antibody and marker quality and concentration) might be different for distinct epitopes and therefore have to be determined separately for every system (Flechler, 2015; Möbius & Posthuma, 2018).

#### 4.4 | Influence of gold particle size on immunolabeling efficiency

As shown in this and in previous studies (e.g., Gu & D'Andrea, 1989; Yokota, 1988), the gold particle size of the detection system was decisive for signal intensity. We obtained the best signal for cells labeled with "ultrasmall" gold. However, the application of "ultrasmall" gold particles involves a number of drawbacks, such as inhomogeneous silver or gold enhancement, and in our case gold particles tended to cluster. In addition, we observed a decreasing binding intensity by increasing size of gold particles from "ultrasmall" gold to 15 nm gold. This was in line with previous results (Horisberger, 1981; Stierhof, Humbel, & Schwarz, 1991). These experiments indicated that obviously a larger number of still unoccupied primary antibodies were left in case of the relatively large gold markers. As a consequence, also antibodies which are bound to smaller fluorescence labels (with enhanced sensitivity) were used for ultrathin resin section labeling (Schwarz & Humbel, 2014). The reduced efficiency of gold markers might be due to electrostatic repulsion (negative surface charge) and steric hindrance arising from gold particles coupled laterally to the F<sub>c</sub>-region of IgG molecules (Supporting Information S1, Dulhunty, Junankar, & Stanhope, 1993). The bigger the gold particle, the larger the steric hindrance and the more difficult it will be for the secondary antibody-gold particle construct to bind to the primary antibody.

#### 4.5 | 3D immunogold labeling

In recent years, there has been huge progress in the field of 3D electron microscopy. The continuous development in sample preparation (from conventional methods to cryo methods), the development of microscopes themselves and the ongoing progress in computing power and visualization tools (e.g., ImageJ, IMOD, and AMIRA<sup>®</sup>), play a decisive role in this context. Current electron microscopy methods that aim to obtain 3D-reconstructions of biological samples comprise serial sectioning including array tomography (Micheva & Smith, 2007),

serial block face-SEM (SBF-SEM), focused ion beam-SEM (FIB-SEM), and tilt-series based (serial-) electron tomography (ET).

Basically, all these methods for 3D-EM could be combined with preembedding and/or postembedding immunocytochemistry, although with some constraints that are inherent to each method. 3D immunolabeling offers two major advantages. First, determination of antigen distribution through a larger volume becomes possible and second, discrimination of specific from unspecific labeling might be achieved easier using quantitative analysis (Müller-Reichert et al., 2003). In this work, 3D-EM was combined with immuno-EM using serial sections of *I. hospitalis* and postembedding labeling of enzymes putatively involved in the carbon fixation pathway of the organism. As expected from the 2D data, gold particles in the 3D model could be preferably observed in the IMC associated with the OCM (Mayer et al., 2012). The labeling pattern of the 3D model once again demonstrated the specificity of immunogold labeling with the ACS-antibody on cells of *Ignicoccus*. Besides the strong signal in the IMC, only few gold particles were found in the cytoplasm. As gold particles in the cytoplasm occurred on almost every section, these labels might also be specific, because they could indicate newly synthesized proteins. These findings were in line with the fact that DNA and ribosomes are located in the cytoplasm, where the ACS needs to be generated (Flechler, 2015; Küper et al., 2010; Mayer et al., 2012).

However, 3D reconstructions of immunolabeled serial sections from whole cells have some disadvantages. Besides a comparably low resolution in *z* (maximum achievable resolution is twice the section thickness; McEwen & Marko, 1998), physically separated sections can show thickness-dependent swelling artifacts, for example, when floating on the surface of the knife's water (Schwarz & Humbel, 1989) or during the labeling procedure. In addition, small angle differences and small deformations because of shrinking by beam damage in the electron microscope can occur (Morphew, 2007). Another limitation of serial section labeling is that antibodies can just bind to the surface of ultrathin resin sections, making gold particles appear as distinct rings around cells in the case of OCM labeling. Furthermore, especially manual segmentation, that is, color-coding of structures and gold particles can be enormously time-consuming. At least for gold particles with a size of 1–6 nm, automatic segmentation might become possible through the introduction of an additional silver- or gold enhancement step.

An alternative for serial section labeling of ultrathin sections is labeling of (serial) semithin sections combined with electron tomography analysis, which benefits from higher resolution in *z* (resin sections: Donohoe, Mogelvang, & Staehelin, 2006; thawed cryosections: Zeuschner et al., 2006). However, the labeling density in *z* is even worse than in 50 nm sections, as the antibodies cannot penetrate the resin. Accordingly, this 3D-method is described to be particularly useful for antigen localization through large volumes (Morphew, 2007). Using immunogold localization of semithin cryosections and electron tomography in 2006, Zeuschner et al. reported on the successful discrimination between COPI and COPII vesicles (which are morphologically indistinguishable in ultrathin cryosections).

For many samples, serial section labeling of ultrathin or semithin sections using TEM analysis with or without tilting the sample,



currently remains the only option to analyze distribution of proteins in a 3D context. Although there are genetic tags available that can be fused to proteins, there is still no genetic system for many nonmodel organisms at present. And although the negative and destructive effects of permeabilization within pre-embedding can be reduced by additional fixation and preparation steps (Humbel, de Jong, Müller, & Verkleij, 1998), it does not appear to be an adequate solution, for example, if well-preserved samples are the goal like in this study.

In addition, serial section labeling is intended for samples such as microorganisms and cell organelles with a size in the  $\mu\text{m}$  range. The results of postsection immunolabeled 3D-reconstructions supported the specificity of immunogold labeling in 2D and provided additional information concerning the spatial distribution of gold particles at least to a certain extent. Specific labeling can be distinguished easier from unspecifically bound gold, if particles occur regularly and on consecutive sections. Finally, localization of proteins might be seen in a different light in an overall cellular context, for example, during immunolabeling experiments with cells of *Ignicoccus*, gold particles were located in vesicles (interpretation of 2D information; also see Junglas et al., 2008), which turned out to be cytoplasmic protrusions after 3D reconstruction (Flechsler, 2015; Heimerl et al., 2017).

## 5 | CONCLUSION

The experiments carried out in this study led to some very interesting suggestions and conclusions. Our results suggest that immunolabeling of Epon-embedded cells can lead to excellent labeling results with a well-preserved ultrastructure. Immunolabeling of methacrylate- and cryosections turned out to be indeed more sensitive, but the preservation of the ultrastructure was compromised.

In our study, we demonstrated that immunocytochemistry experiments of high-pressure-frozen and freeze-substituted samples containing around 0.2%  $\text{OsO}_4$  could be successful. The application of  $\text{OsO}_4$  during freeze substitution helped to fix and to retain components containing C–C double bonds. This resulted in a significant better structural preservation.

Furthermore, the application of an accelerated protocol for immunolabeling on sections showed that an incubation time of 30 min for each antibody suffices. In addition, shorter incubation times helped to better preserve structural details.

As described in previous studies, the smaller the gold particle coupled to a secondary antibody, the stronger the signal intensity. And finally, 3D reconstructions from immunolabeled serial sections were suitable for samples with small volumes and provided additional information regarding the spatial distribution of gold particles in the sample.

## ACKNOWLEDGMENTS

We wish to thank Heinz Schwarz for fruitful discussions and guidance in difficult times. Furthermore, we thank Christine Maßen, Marion Debus, Jennifer Grünert, Perla Ileana Montes De Oca Reyes and Cornelia Niemann for technical assistance, Franziska Hempel and Uwe-G. Maier for scientific support, and Christoph Trieb for artwork.

## CONFLICT OF INTEREST

All contributing authors state that there is no conflict of interest.

## ORCID

Andreas Klingl  <https://orcid.org/0000-0001-8414-8317>

## REFERENCES

- Ainsworth, S., & Karnovsky, M. (1972). An ultrastructural staining method for enhancing the size and electron opacity of ferritin in thin sections. *Journal of Histochemistry and Cytochemistry*, 20(3), 225–229.
- Baschong, W., Baschong-Priscianotto, C., Wurtz, M., Carlemalm, E., Kellenberger, C., & Kellenberger, E. (1984). Preservation of protein structures for electron microscopy by fixation with aldehydes and/or  $\text{OsO}_4$ . *European Journal of Cell Biology*, 35, 2126.
- Behrman, E. J. (1984). The chemistry of osmium tetroxide fixation. In J. P. Revel, T. Barnard, & G. H. Haggis (Eds.), *The Science of Biological Specimen Preparation 1983* (pp. 1–5). IL: AMF O'Hare, SEM Inc..
- Berryman, M. A., Porter, W. R., Rodewald, R. D., & Hubbard, A. L. (1992). Effects of tannic acid on antigenicity and membrane contrast in ultrastructural immunocytochemistry. *Journal of Histochemistry and Cytochemistry*, 40, 845–857.
- Berryman, M. A., & Rodewald, R. D. (1990). An enhanced method for post-embedding immunocytochemical staining which preserves cell membranes. *Journal of Histochemistry and Cytochemistry*, 38, 159–170.
- Dahl, R., & Staehelin, L. A. (1989). High-pressure-freezing for the preservation of biological structure: theory and practice. *Journal of Electron Microscopy*, 13, 165–174.
- Danscher, G. (1981). Localization of gold in biological tissue. A photochemical method for light and electron microscopy. *Histochemistry* 71(1): 81–88.
- Donohoe, B. S., Mogelvang, S., & Staehelin, L. A. (2006). Electron tomography of ER, Golgi and related membrane systems. *Methods*, 39, 154–162.
- Dulhunty, A. F., Junankar, P. R., & Stanhope, C. (1993). Immunogold labeling of calcium ATPase in sarcoplasmic reticulum of skeletal muscle: use of 1-nm, 5-nm, and 10-nm gold. *Journal of Histochemistry & Cytochemistry*, 41, 1459–1466.
- Dutton, A. H., Tokuyasu, K., & Singer, S. (1979). Iron dextran antibody conjugates: General method for simultaneous staining of two components in high-resolution immunoelectron microscopy. *Proceedings of the National Academy of Sciences*, 76(7), 3392–3396.
- Faulk, W. P., & Taylor, G. M. (1971). An immunocolloid method for the electron microscope. *Immunocytochemistry*, 8, 1081–1083.
- Flechsler, J. (2015). *A study on the  $\text{CO}_2$  fixation pathway of Ignicoccus hospitalis*. (Doctoral dissertation), University of Regensburg, Regensburg, Germany. urn:nbn:de:bvb:355-epub-327021
- Frankl, A., Mari, M., & Reggiori, F. (2015). Electron microscopy for ultrastructural analysis and protein localization in *Saccharomyces cerevisiae*. *Microbial Cell*, 2(11), 412–428. <https://doi.org/10.15698/mic2015.11.237>
- Griffith, J., Mari, M., De Mazière, A., & Reggiori, F. (2008). A cryosectioning procedure for the ultrastructural analysis and the immunogold labeling of yeast *Saccharomyces cerevisiae*. *Traffic*, 9(7), 1060–1072. <https://doi.org/10.1111/j.1600-0854.2008.00753.x>
- Griffiths, G. (1993). *Fine Structure Immunocytochemistry* (1st ed.). Berlin, Heidelberg: Springer Verlag.
- Griffiths, G., McDowall, A., Back, R., & Dubochet, J. (1984). On the preparation of cryosections for immunocytochemistry. *Journal of Ultrastructure Research*, 89, 65–78.
- Groos, S., Reale, E., & Luciano, L. (2001). Re-evaluation of epoxy resin sections for light and electron microscopic immunostaining. *Journal of Histochemistry and Cytochemistry*, 49(3), 397–406. <https://doi.org/10.1177/002215540104900313>

- Gu, J., & D'Andrea, M. (1989). Comparison of detecting sensitivities of different sizes of gold particles with electron-microscopic immunogold staining using atrial natriuretic peptide in rat atria as a model. *American Journal of Anatomy*, 185, 264–270.
- Heimerl, T., Flechslers, J., Pickl, C., Heinz, V., Salecker, B., Zweck, J., ... Rachel, R. (2017). A complex endomembrane system in the Archaeon *Ignicoccus hospitalis* tapped by *Nanoarchaeum equitans*. *Frontiers in Microbiology*, 8, 1072.
- Hempel, F., Lau, J., Klingl, A., & Maier, U. G. (2011). Algae as protein factories: expression of a human antibody and the respective antigen in the diatom *Phaeodactylum tricornutum*. *PLoS One*, 6, e28424.
- Hobot, J. A. (1990). New aspects of bacterial ultrastructure as revealed by modern acrylics for electron microscopy. *Journal of Structural Biology*, 104, 169–177.
- Hopwood, D. (1969). Fixation of proteins by osmium tetroxide, potassium dichromate and potassium permanganate. model experiments with bovine serum albumin and bovine gamma-globulin. *Histochemie*, 18, 250–260.
- Horisberger, M. (1981). Colloidal gold: a cytochemical marker for light and fluorescent microscopy and for transmission and scanning electron microscopy. *Scanning Electron Microscopy*, 1981(Pt 2), 9–31.
- Horowitz, R. A., Giannasca, P. J., & Woodcock, C. L. (1990). Ultrastructural preservation of nuclei and chromatin: improvement with low-temperature methods. *Journal of Microscopy*, 157, 205–224.
- Humbel, B. A., de Jong, M. D., Müller, W. H., & Verkleij, A. J. (1998). Pre-embedding immunolabeling for electron microscopy: an evaluation of permeabilization methods and markers. *Microscopy Research and Technique*, 42(1), 43–58.
- Humbel, B. M., & Schwarz, H. (1989). Freeze-substitution for immunocytochemistry. In A. J. Cerkleij & J. L. M. Leunissen (Eds.), *Immuno-gold labeling in cell biology* (p. 115). Boca Raton, FL: CRC Press.
- Hyatt, A. D. (1991). Immunogold labelling techniques. In J. R. Harris (Ed.), *Electron microscopy in Biology: A practical approach* (pp. 59–81). Oxford, UK: IRL Press of Oxford University Press.
- Junglas, B., Briegel, A., Burghardt, T., Walther, P., Wirth, R., Huber, H., & Rachel, R. (2008). *Ignicoccus hospitalis* and *Nanoarchaeum equitans*: ultrastructure, cell-cell interaction, and 3D reconstruction from serial sections of freeze-substituted cells and by electron cryotomography. *Archives of Microbiology*, 190(3), 395–408. <https://doi.org/10.1007/s00203-008-0402-6>
- Kellenberger, E., Dürrenberger, M., Villiger, W., Carlemalm, E., & Wurtz, M. (1987). The efficiency of immunolabel on lowicryl sections compared to theoretical predictions. *Journal of Histochemistry and Cytochemistry*, 35, 959–969.
- Kenneth, M., Travors, P., & Walport, M. (2008). *Janeway's Immunobiology*. Garland Science (7th ed.). Taylor and Francis Group, New York.
- Küper, U., Meyer, C., Müller, V., Rachel, R., & Huber, H. (2010). Energized outer membrane and spatial separation of metabolic processes in the hyperthermophilic archaeon *Ignicoccus hospitalis*. *Proceedings of the National Academy of Sciences of the United States of America*, 107, 3152–3156.
- Lehtrekk, K. F., Teltenkötter, A., & Grunow, A. (1999). A 210 kDa protein is located in a membrane microtubule linker at the distal end of mature and nascent basal bodies. *Journal of Cell Science*, 112, 1633–1644.
- Liou, W., Geuze, H. J., & Slot, J. W. (1996). Improving structural integrity of cryosections for immunogold labeling. *Histochemistry and Cell Biology*, 106(1), 41–58.
- Liu, X., Hempel, F., Stork, S., Bolte, K., Moog, D., Heimerl, T., ... Zauner, S. (2016). Addressing various compartments of the diatom model organism *Phaeodactylum tricornutum* via sub-cellular marker proteins. *Algal Research*, 20, 249–257. <https://doi.org/10.1016/j.algal.2016.10.018>
- Locke, M. (1994). Preservation and contrast without osmication or section staining. *Microscopy Research and Technique*, 29, 1–10.
- Luft, J. H. (1961). Improvements in epoxy resin embedding methods. *Journal of Biophysical and Biochemical Cytology*, 9, 409–414.
- Maupin, P., & Pollard, T. D. (1983). Improved preservation and staining of HeLa cell actin filaments, clathrin-coated membranes, and other cytoplasmic structures by tannic acid-glutaraldehyde-saponin fixation. *Journal of Cell Biology*, 96(1), 51–62.
- Maupin-Szamiar, P., & Pollard, T. D. (1978). Actin filament destruction by osmium tetroxide. *Journal of Cell Biology*, 77(3), 837–852.
- Mayer, F., Küper, U., Meyer, C., Daxer, S., Müller, V., Rachel, R., & Huber, H. (2012). Amp-forming acetyl coenzyme A synthetase in the outermost membrane of the hyperthermophilic crenarchaeon *Ignicoccus hospitalis*. *Journal of Bacteriology*, 194, 1572–1581.
- McDonald, K. L. (2014). Out with the old and in with the new: rapid specimen preparation procedures for electron microscopy of sectioned biological material. *Protoplasma*, 251, 429–448.
- McEwen, B. F., & Marko, M. (1998). Chapter 5: Three-dimensional transmission electron microscopy and its application to mitosis research. *Methods in Cell Biology*, 61, 81–111. [https://doi.org/10.1016/S0091-679X\(08\)61976-7](https://doi.org/10.1016/S0091-679X(08)61976-7)
- Meyer, C., Heimerl, T., Wirth, R., Klingl, A., & Rachel, R. (2014). The iho670 fibers of *Ignicoccus hospitalis* are anchored in the cell by a spherical structure located beneath the inner membrane. *Journal of Bacteriology*, 196, 3807–3815.
- Micheva, K. D., & Smith, S. J. (2007). Array tomography: a new tool for imaging the molecular architecture and ultrastructure of neural circuits. *Neuron*, 55(1), 25–36.
- Mix, A.-K., Cenci, U., Heimerl, T., Marter, P., Wirkner, M.-L., & Moog, D. (2018). Identification and localization of peroxisomal proteins indicates the presence of peroxisomes in the cryptophyte *Guillardia theta* and other "chromalveolates". *Genome Biology and Evolution*, 10(10), 2834–2852. <https://doi.org/10.1093/gbe/evy214>
- Miyake, J. A., & Colquhoun, A. (2012). Electron microscopy and immunogold labelling of proteins involved in brain tumour growth and invasion. In A. Méndez-Vilas (Ed.), *Current Microscopy Contributions to Advances in Science and Technology*. Badajoz: Formatex Research Center.
- Möbius, W., & Posthuma, G. (2018). Sugar and ice: Immunoelectron microscopy using cryosections according to the tokuyasu method. *Tissue and Cell*, 57, 90–102. <https://doi.org/10.1016/j.tice.2018.08.010>
- Moor, H. & Riehle, U. (1968). *Snap-freezing under high pressure: a new fixation technique for freeze-etching*. Proceedings of the 4th International Conference on Electron Microscopy, Vol. 2, pp. 33–34.
- Morphew, M. K. (2007). 3D immunolocalization with plastic sections. *Methods in Cell Biology*, 79, 493–513.
- Moussian, B., Tang, E., Tønning, A., Helms, S., Schwarz, H., Nüsslein-Volhard, C., & Uv, A. E. (2006). *Drosophila* Knickkopf and Retroactive are needed for epithelial tube growth and cuticle differentiation through their specific requirement for chitin filament organization. *Development*, 133, 163–171.
- Müller-Reichert, T., Sassoon, I., O'Toole, E., Romao, M., Ashford, A. J., Hyman, A. A., & Antony, C. (2003). Analysis of the distribution of the kinetochore protein ndc10p in *Saccharomyces cerevisiae* using 3-d modeling of mitotic spindles. *Chromosoma*, 111, 417–428.
- Nakane, P. K., & Pierce, G. B. (1967). Enzyme-labeled antibodies for the light and electron microscopic localization of tissue antigens. *The Journal of Cell Biology*, 33, 307–318.
- Ndinyanka Fabrice, T., Kaech, A., Barmettler, G., Eichenberger, C., Knox, J. P., Grossniklaus, U., & Ringli, C. (2017). Efficient preparation of *Arabidopsis* pollen tubes for ultrastructural analysis using chemical and cryo-fixation. *BMC Plant Biology*, 17(1), 176. <https://doi.org/10.1186/s12870-017-1136-x>
- Newman, G. R., & Hobot, J. A. (1999). Resins for combined light and electron microscopy: a half century of development. *The Histochemical Journal*, 31, 495–505.
- Ottersen, O. P., Zhang, N., & Walberg, F. (1992). Metabolic compartmentation of glutamate and glutamine: morphological evidence obtained by



- quantitative immunocytochemistry in rat cerebellum. *Neuroscience*, 46, 519–534.
- Paper, W., Jahn, U., Hohn, M. J., Kronner, M., Näther, D. J., Burghardt, T., ... Huber, H. (2007). *Ignicoccus hospitalis* sp. nov., the host of 'Nanoarchaeum equitans'. *International Journal of Systematic and Evolutionary Microbiology*, 57, 803–808.
- Pedersen, L. B., Geimer, S., & Rosenbaum, J. L. (2006). Dissecting the molecular mechanisms of intraflagellar transport in *Chlamydomonas*. *Current Biology*, 16, 450–459.
- Peschke, M., Moog, D., Klingl, A., Maier, U. G., & Hempel, F. (2013). Evidence for glycoprotein transport into complex plastids. *Proceedings of the National Academy of Sciences of the United States of America*, 110, 10860–10865.
- Peters, P. J., Bos, E., & Griekspoor, A. (2006). Cryo-immunogold electron microscopy. In *Current Protocols in Cell Biology*. John Wiley & Sons, New Jersey.
- Rachel, R., Meyer, C., Klingl, A., Gürster, S., Heimerl, T., Wasserburger, N., ... Wanner, G. (2010). Analysis of the ultrastructure of archaea by electron microscopy. *Methods in Cell Biology*, 96, 47–69.
- Richards, R. G., Owen, G. R., Riehle, M., Gwynn, A., & Curtis, A. S. G. (2001). Immunogold labelling of fibroblast focal adhesion sites visualised in fixed material using scanning electron microscopy, and living, using internal reflection microscopy. *Cell Biology International*, 25(12), 1237–1249.
- Richter, S., Müller, L. M., Stierhof, Y.-D., Mayer, U., Takada, N., Kost, B., ... Jürgens, G. (2012). Polarized cell growth in *Arabidopsis* requires endosomal recycling mediated by GBF1-related ARF exchange factors. *Nature Cell Biology*, 14, 80–86. <https://doi.org/10.1038/ncb2389>
- Romano, E. L., & Romano, M. (1977). Staphylococcal protein a bound to colloidal gold: a useful reagent to label antigen-antibody sites in electron microscopy. *Immunochemistry*, 14(9–10), 711–715.
- Roth, J., Bendayan, M., & Orci, L. (1978). Ultrastructural localization of intracellular antigens by the use of protein a-gold complex. *Journal of Histochemistry and Cytochemistry*, 26, 1074–1081.
- Schreiber, V., Dersch, J., Puzik, K., Bäcker, O., Liu, X., Stork, S., ... Maier, U. G. (2017). The central vacuole of the diatom *Phaeodactylum tricornutum*: Identification of new vacuolar membrane proteins and a functional di-leucine based targeting motif. *Protist*, 168(3), 271–282. <https://doi.org/10.1016/j.protis.2017.03.001>
- Schneider, C. A., Rasant, W. S., & Eliceiri, K. W. (2012). NIH Image to ImageJ: 25 years of image analysis. *Nature Methods* 9(7): 671–675.
- Schwarz, H., & Hohenberg, H. (2001). Immuno-electron microscopy. *eLS*. <https://doi.org/10.1038/ngp.els.0003000>
- Schwarz, H., & Humbel, B. M. (1989). Influence of fixatives and embedding media on immunolabelling of freeze-substituted cells. *Scanning Microscopy Supplement*, 3, 57–63.
- Schwarz, H., & Humbel, B. M. (2014). Correlative light and electron microscopy using immunolabeled sections. In J. Kuo (Ed.), *Electron Microscopy. Methods in Molecular Biology (Methods and Protocols)* (Vol. 1117, pp. 559–592). Humana Press, Totowa, NJ. [https://doi.org/10.1007/978-1-62703-776-1\\_25](https://doi.org/10.1007/978-1-62703-776-1_25)
- Shiurba, R. (2001). Freeze-substitution: origins and applications. *International Review of Cytology*, 206, 45–96.
- Singer, S., & Schick, A. F. (1961). The properties of specific stains for electron microscopy prepared by the conjugation of antibody molecules with ferritin. *The Journal of Cell Biology*, 9(3), 519–537.
- Slot, J. W., & Geuze, H. J. (1985). A new method of preparing gold probes for multiple-labelling cytochemistry. *European Journal of Cell Biology*, 38(1), 87–93.
- Steinbrecht, R. A., & Müller, M. (1987). Freeze substitution and freeze drying. In R. A. Steinbrecht & K. Zirold (Eds.), *Cryo Techniques in Biological Electron Microscopy* (pp. 149–172). Berlin: Springer-Verlag.
- Stierhof, Y.-D., Hermann, R., Humbel, B. M., & Schwarz, H. (1995). Use of TEM, SEM, and STEM in imaging 1 nm colloidal gold particles. In M. A. Hayat (Ed.), *Immunogold-silver staining: principles, methods, and applications* (pp. 97–118). Boca Raton, FL: CRC Press.
- Stierhof, Y. D., Humbel, B. M., & Schwarz, H. (1991). Suitability of different silver enhancement methods applied to 1 nm colloidal gold particles: an immunoelectron microscopic study. *Journal of Electron Microscopy Technique*, 17(3), 336–343.
- Stierhof, Y. D., & Schwarz, H. (1989). Labeling properties of sucrose-infiltrated cryosections. *Scanning Microscopy Supplement*, 3, 35–46.
- Stirling, J. W. (1990). Immuno- and affinity probes for electron microscopy: a review of labeling and preparation techniques. *Journal of Histochemistry and Cytochemistry*, 38, 145–157.
- Studer, D., Graber, W., Al-Amoudi, A., & Egli, P. (2001). A new approach for cryofixation by high-pressure freezing. *Journal of Microscopy*, 203(3), 285–294.
- Tokuyasu, K. T. (1973). A technique for ultracryotomy of cell suspensions and tissues. *The Journal of Cell Biology*, 57, 551–565.
- Valentino, K. L., Crumrine, D. A., & Reichardt, L. F. (1985). Lowicryl K4M embedding of brain tissue for immunogold electron microscopy. *Journal of Histochemistry and Cytochemistry*, 33, 969–973.
- Viens, A., Harper, F., Pichard, E., Comisso, M., Pierron, G., & Ogryzko, V. (2008). Use of protein biotinylation in vivo for immunoelectron microscopic localization of a specific protein isoform. *Journal of Histochemistry and Cytochemistry*, 56(10), 911–919. <https://doi.org/10.1369/jhc.2008.951624>
- Webster, P., & Webster, A. (2014). Cryosectioning fixed and cryoprotected biological material for immunocytochemistry. *Methods in Molecular Biology*, 1117, 273–313. [https://doi.org/10.1007/978-1-62703-776-1\\_13](https://doi.org/10.1007/978-1-62703-776-1_13)
- Winter, G., Fuchs, M., McConville, M. J., Stierhof, Y. D., & Overath, P. (1994). Surface antigens of *Leishmania mexicana* amastigotes: characterization of glycoinositol phospholipids and a macrophage-derived glycosphingolipid. *Journal of Cell Science*, 107(9), 2471–2482.
- Yokota, S. (1988). Effect of particle size on labeling density for catalase in protein a-gold immunocytochemistry. *Journal of Histochemistry and Cytochemistry*, 36, 107–109.
- Zeuschner, D., Geerts, W. J. C., van Donselaar, E., Humbel, B. M., Slot, J. W., Koster, A. J., & Klumperman, J. (2006). Immuno-electron tomography of ER exit sites reveals the existence of free COPII-coated transport carriers. *Nature Cell Biology*, 8, 377–383.

## SUPPORTING INFORMATION

Additional supporting information may be found online in the Supporting Information section at the end of this article.

**How to cite this article:** Flechslers J, Heimerl T, Pickl C, Rachel R, Stierhof Y-D, Klingl A. 2D and 3D immunogold localization on (epoxy) ultrathin sections with and without osmium tetroxide. *Microsc Res Tech*. 2020;83:691–705. <https://doi.org/10.1002/jemt.23459>